Seasonal variations in N_2O emissions from central California

Seongeun Jeong,[1] Chuanfeng Zhao,[1,2] Arlyn E. Andrews,[3] Edward J. Dlugokencky,[3] Colm Sweeney,[3,4] Laura Bianco,[3,4] James M. Wilczak,[3] and Marc L. Fischer[1]

Received 8 May 2012; revised 16 July 2012; accepted 23 July 2012; published 31 August 2012.

[1] We estimate nitrous oxide (N_2O) emissions from Central California for the period of December 2007 through November 2009 by comparing N_2O mixing ratios measured at a tall tower (Walnut Grove, WGC) with transport model predictions based on two global *a priori* N_2O emission models (EDGAR32 and EDGAR42). Atmospheric particle trajectories and surface footprints are computed using the Weather Research and Forecasting (WRF) and Stochastic Time-Inverted Lagrangian Transport (STILT) models. Regression analyses show that the slopes of predicted on measured N_2O from both emission models are low, suggesting that actual N_2O emissions are significantly higher than the EDGAR inventories for all seasons. Bayesian inverse analyses of regional N_2O emissions show that posterior annual N_2O emissions are larger than both EDGAR inventories by factors of 2.0 ± 0.4 (EDGAR32) and 2.1 ± 0.4 (EDGAR42) with seasonal variation ranging from 1.6 ± 0.3 to 2.5 ± 0.4 for an influence region of Central California within approximately 150 km of the tower. These results suggest that if the spatial distribution of N_2O emissions in California follows the EDGAR emission models, then actual emissions are 2.7 ± 0.5 times greater than the current California emission inventory, and total N_2O emissions account for $8.1 \pm 1.4\%$ of total greenhouse gas emissions from California. **Citation:** Jeong, S., C. Zhao, A. E. Andrews, E. J. Dlugokencky, C. Sweeney, L. Bianco, J. M. Wilczak, and M. L. Fischer (2012), Seasonal variations in N_2O emissions from central California, *Geophys. Res. Lett.*, *39*, L16805, doi:10.1029/2012GL052307.

1. Introduction

[2] Nitrous oxide (N_2O) ranks as the third most important long-lived greenhouse gas (GHG) from a regulatory perspective behind CH_4 and CO_2 [*Hofmann et al.*, 2006; *Montzka et al.*, 2011] based on changes in the amount of N_2O in the atmosphere since the start of the industrial revolution, its long atmospheric residence time (~110 years), and its ability to absorb infrared radiation. Given the significance of N_2O as a GHG it is important to be able to quantify changes in emissions. A recent study showed that a large portion of the increase in global atmospheric N_2O can be attributed to the use of fertilizers [*Park et al.*, 2012]. However, current process-level understanding and driving data are not sufficient to accurately predict N_2O emissions from the multiple sources. Thus, there are large uncertainties in estimating N_2O emissions using bottom-up models. Inversions which use concentration changes in N_2O and transport to infer sources provide an effective tool for understanding N_2O emissions. Correspondingly, attention has focused on inverse model assessment of global [*Huang et al.*, 2008; *Hirsch et al.*, 2006], and regional [*Kort et al.*, 2008; *Corazza et al.*, 2011] N_2O sources.

[3] California currently emits approximately 500 Tg of CO_2 equivalent (CO_2 eq) GHGs per year (100-year global warming potential (GWP) = 310 g CO_2 eq/g N_2O [*IPCC*, 1995]), with N_2O currently estimated to contribute ~3% of the total [*California Air Resources Board* (*CARB*), 2012]. However, regional N_2O emission estimates are likely uncertain by at least 50% [*National Research Council*, 2010]. California has committed to an ambitious plan to reduce GHG emissions to 1990 levels by 2020 through Assembly Bill 32 (AB32). Verifying the success of emission control strategies will require quantitative accounting for current and future GHG emissions including N_2O. Despite the importance of regional verification of N_2O emissions, measurements have yet to constrain seasonal or regional N_2O emissions from California.

[4] In this paper, we quantify N_2O emissions from Central California using measurements of N_2O from daily discrete air samples collected from December 2007 to November 2009 within a Bayesian inverse modeling framework, the first analysis of seasonal variations in N_2O emissions from the mixed urban and rural area of Central California.

2. Methods

2.1. Measurements

[5] In 2008 and 2009, air samples were collected nearly daily at 91 m above the surface from a tall tower near Walnut Grove (WGC), California (lat = 38.27°N, lon = 121.49°W) as part of the NOAA Global Monitoring Division, Carbon Cycle Groups' tall tower measurement program (www.esrl.noaa.gov/gmd/ccgg/towers/). The approximately 2 liter samples were each collected during a two-minute period within a few minutes of 2200 GMT (1400 local time, LT). N_2O dry-air mole fractions were subsequently measured using gas chromatography with electron capture detection relative to NOAA's N_2O standard scale [*Hall et al.*, 2007] with a repeatability of 0.4 ppb (68% confidence interval).

[1]Environmental Energy Technologies Division, Lawrence Berkeley National Laboratory, Berkeley, California, USA.
[2]Atmospheric, Earth and Energy Division, Lawrence Livermore National Laboratory, Livermore, California, USA.
[3]Earth System Research Laboratory, NOAA, Boulder, Colorado, USA.
[4]Cooperative Institute for Research in Environmental Sciences, University of Colorado at Boulder, Boulder, Colorado, USA.

Corresponding author: S. Jeong, Environmental Energy Technologies Division, Lawrence Berkeley National Laboratory, MS 90K-127 1 Cyclotron Rd., Berkeley, CA 94720, USA. (sjeong@lbl.gov)

These samples were analyzed on the same analytical systems used for weekly discrete samples collected from NOAA's Global Cooperative Air Sampling network (www.esrl.noaa.gov/gmd/ccgg/flask.html).

2.2. Footprint Simulations

[6] Predicted contributions to N_2O mixing ratios from emissions within the modeling domain are calculated as **FE**, where **F** is the footprint, which represents the sensitivity of the receptor to surface influences, and **E** is the *a priori* emissions. Footprints are calculated using the Stochastic Time-Inverted Lagrangian Transport (STILT) model [*Lin et al.*, 2003]. In this study, 500 particles are released from the WGC tower at the time of each air sample and transported backward in time 5–7 days to insure a majority of the particles reach positions representative of the background conditions relative to the California region. The meteorology used to drive this transport model is simulated by the Weather Research and Forecasting (WRF2.2) model [*Skamarock et al.*, 2005], which has been slightly modified to be coupled with STILT [*Nehrkorn et al.*, 2010] (see the auxiliary material).[1]

2.3. *A Priori* Emissions

[7] We use EDGAR 32FT2000 (henceforth EDGAR32) [*Olivier et al.*, 2005] and EDGAR version 4.2 (EDGAR42) (European Commission Joint Research Centre (JRC) and Netherlands Environmental Assessment Agency, Emission Database for Global Atmospheric Research (EDGAR), release version 4.2, 2011, http://edgar.jrc.ec.europa.eu) *a priori* emission maps (see the auxiliary material) to represent surface emission sources and sinks for N_2O at different spatial resolutions (1.0° and 0.1°, respectively). The EDGAR inventory includes all anthropogenic sources of N_2O; emissions are constant in time, without seasonality. The annual total emission for California from EDGAR32 and EDGAR42 is 21.6 and 20.0 Tg CO_2 eq, respectively. Both EDGAR inventories list emissions that are higher than the current CARB inventory (16 Tg CO_2 eq) [*CARB*, 2012]. In terms of spatial distribution at the sub-regional scale, annual emission sums for Regions 6, 7 and 8 near the WGC tower (see the auxiliary material for region classification) from EDGAR32 are 1.6, 2.8, 1.4 Tg CO_2 eq, which are similar to those of EDGAR42: 1.3, 2.7, and 1.4 Tg CO_2 eq. As in *Kort et al.* [2008], we assume that N_2O emissions from unfertilized natural soils are small (see details in the auxiliary material) compared to emissions from agricultural soils and other anthropogenic sources in California. In this regard, N_2O emissions from fertilized forest soils are included in EDGAR42.

2.4. Inverse Method

[8] We apply a scaling factor Bayesian inverse (SFBI) method to estimate N_2O emissions from Central California using N_2O measured at WGC. The local measured mixing ratios, **c**, are calculated by subtracting a boundary condition mixing ratio, representing the estimated mixing ratio of air entering the domain (see the auxiliary material). As described in *Gerbig et al.* [2003], *Zhao et al.* [2009] and *Jeong et al.* [2012], **c** can be modeled as

$$\mathbf{c} = \mathbf{K}\boldsymbol{\lambda} + \mathbf{v} \quad (1)$$

with an analytical solution for $\boldsymbol{\lambda}$ as

$$\boldsymbol{\lambda}_{post} = \left(\mathbf{K}^T\mathbf{R}^{-1}\mathbf{K} + \mathbf{Q}_\lambda^{-1}\right)^{-1}\left(\mathbf{K}^T\mathbf{R}^{-1}\mathbf{c} + \mathbf{Q}_\lambda^{-1}\boldsymbol{\lambda}_{prior}\right) \quad (2)$$

where $\mathbf{K} = \mathbf{FE}$, $\boldsymbol{\lambda}$ is a state vector for scaling factors, **v** is a vector representing the model-measurement mismatch with a covariance matrix **R**, $\boldsymbol{\lambda}_{\text{prior}}$ is the *a priori* estimate for $\boldsymbol{\lambda}$, and $\mathbf{Q}_\lambda$ is the error covariance associated with $\boldsymbol{\lambda}_{\text{prior}}$. The posterior error covariance for $\boldsymbol{\lambda}$, $\mathbf{V}_{\text{post}}$, is $(\mathbf{K}^T\mathbf{R}^{-1}\mathbf{K} + \mathbf{Q}_\lambda^{-1})^{-1}$. We apply the SFBI method at the monthly scale ($\boldsymbol{\lambda} = 13 \times 1$ vector for each month) to resolve seasonal variations. Data for the same month from 2008 and 2009 are combined, yielding 30–60 data points depending on the availability of flask measurements. *National Research Council* [2010] reported that N_2O emission estimate uncertainties for agricultural soils and manure management range from 10% to more than 100%. Because the Central California region includes large N_2O emission sources such as agriculture fertilizers and livestock [*Park et al.*, 2012], we use 100% uncertainty in our *a priori* emission models.

[9] Following *Bergamaschi et al.* [2005] and *Jeong et al.* [2012], outliers are removed after the initial inversion to avoid biases that might be introduced by the outliers. The second (final) inversion uses data that are accepted by applying the selection criteria $|\mathbf{c}_i - (\mathbf{K}\boldsymbol{\lambda})_i|^2 < \alpha\mathbf{R}_i$, where α is a fixed value within each month. As in the first inversion, the final inversion is performed using the original *a priori* emission maps. The value of α for each month is chosen such that the chi-square values from the final inversion are close to unity [*Tarantola*, 1987] and ranges between 1.7 and 3 in this study.

2.5. Uncertainty Analysis

[10] Along with $\mathbf{Q}_\lambda$, the model-measurement mismatch covariance **R** controls the relative weighting of the prior flux estimates and the data in the inversion. In our study that uses daily air samples, the temporal correlation is expected to be weak as *Lin and Gerbig* [2005] showed that the correlation timescale for wind errors is less than 3 hours. Therefore, following *Gerbig et al.* [2003], *Zhao et al.* [2009], *Göckede et al.* [2010], and *Jeong et al.* [2012] the diagonal elements of **R** (off-diagonal elements equal to zero) are estimated from the linear sum of contributing uncertainties as

$$\mathbf{R}_i = \mathbf{S}_{\text{bkgd}} + \mathbf{S}_{\text{transPBL}} + \mathbf{S}_{\text{transWIND}} + \mathbf{S}_{\text{part}} + \mathbf{S}_{\text{aggr}}. \quad (3)$$

[11] Details for error sources are explained in the auxiliary material, and we describe them briefly below.

[12] The background uncertainty ($\mathbf{S}_{\text{bkgd}}$) is estimated by comparing two marine boundary layer background data sets available for 2008: (1) latitudinally averaged marine boundary layer N_2O background (a 2-dimensional look-up table), and (2) latitudinally averaged 3-dimensional N_2O curtain for eight different vertical levels (see the auxiliary material for details). Uncertainty estimates in background N_2O are 0.38, 0.46, 0.24, and 0.28 ppb (henceforth, all errors reported at 68% confidence) for spring, summer, fall, and winter, respectively. Uncertainty in predicted N_2O signals due to errors in modeled planetary boundary layer (PBL) height ($\mathbf{S}_{\text{transPBL}}$) is estimated by comparing PBL heights (*Zi*) from WRF with measured *Zi* at wind profiler stations near the WGC tower as in *Zhao et al.* [2009] and *Jeong et al.*

[1] Auxiliary materials are available in the HTML. doi:10.1029/2012GL052307.

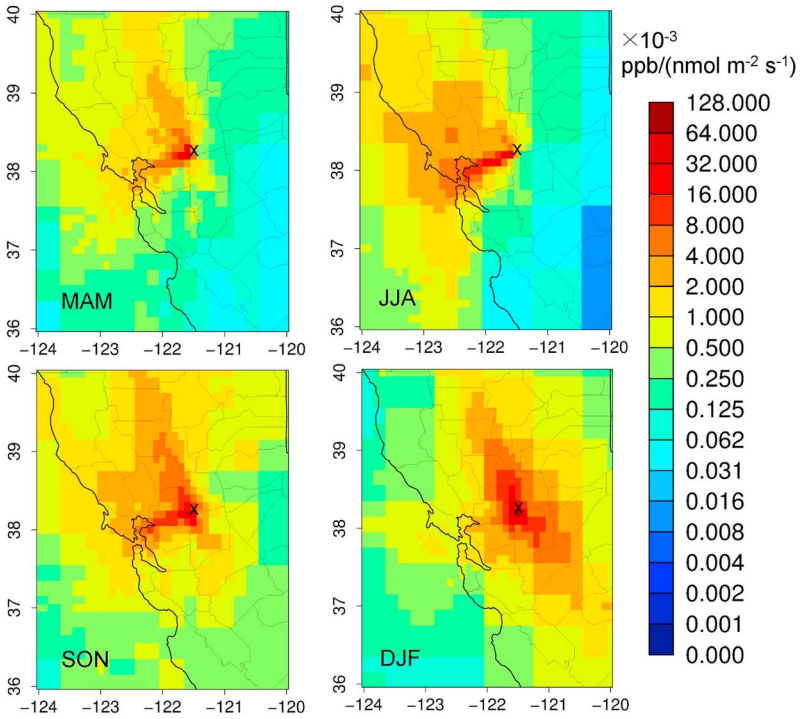

Figure 1. Seasonally averaged footprints during the afternoon hours for spring (March, April, May), summer (June, July, August), fall (September, October, November), and winter (December, January, February). Footprints are shown focusing on Regions 6, 7 and 8, which are sensitive to the WGC tower (black "x").

[2012]. We estimate uncertainties of 0.05, 0.03, 0.27, and 0.49 ppb for spring, summer, fall and winter, respectively. Uncertainty in modeled N_2O signals due to errors in modeled winds ($\mathbf{S}_{\text{transWIND}}$) is estimated using modeled and measured winds for the 127 m height on the WGC tower. Following the experiment with CH_4 signals [*Jeong et al.*, 2012], we adopt 10% of the mean signal level for the wind uncertainty. For the uncertainties due to the particle number ($\mathbf{S}_{\text{part}}$) and aggregation error ($\mathbf{S}_{\text{aggr}}$), we use 5% and 11% of the mean signal level respectively, following *Jeong et al.* [2012]. Finally, the uncertainties were combined in quadrature to yield total model-data mismatch estimates of 0.40, 0.48, 0.41, and 0.63 ppb for spring, summer, fall and winter, respectively. Seasonally estimated model-data mismatch uncertainties are used for all the months belonging to the given season.

3. Results

3.1. Footprints

[13] Figure 1 shows the average footprints for spring, summer, fall, and winter in 2008–2009. The footprints for each season were averaged during the afternoon hours when measurements were available, mostly at 1400 LT. There is a clear seasonal pattern for the distribution of footprints, which is important to attribute signals to different emission sources for each season. The summer footprints are strongest from the San Francisco Bay area to the west of the WGC tower due to the dominance of land-ocean winds. In the transition seasons of spring and fall, footprints are also strong in the North Central Valley due to a shift toward north-south winds. The winter footprints are strongest in the Central Valley, while reaching the northern San Joaquin Valley. The spatial distribution of footprints for the four seasons shows that tower measurements are sensitive to Regions 6, 7, and 8, and our inverse analysis focuses on these three regions where a large reduction in posterior uncertainties is obtained.

3.2. Linear Regression Analysis

[14] We compare predicted and measured local N_2O signals at WGC using a chi-squared (fitexy) linear regression analysis [*Press et al.*, 1992] that considers uncertainties in parameters of both axes. Table 1 summarizes the results obtained from regression analyses for each month between December 2007 and November 2009. The slopes of predicted on measured N_2O from both emission models are generally less than 1, while showing some seasonal variation. The low slopes suggest that actual N_2O emissions are significantly higher than the EDGAR inventory. The linear analysis result also suggests that there is no significant difference between EDGAR32 and EDGAR42 as one might expect from the regional N_2O sums and their spatial distribution (see Section 2.3). A linear analysis based on continuous N_2O measurements at WGC during April 2010 showed a similar result with a slope of 0.34 ± 0.05 (see the auxiliary material).

3.3. Bayesian Inverse Analysis

[15] Posterior predicted N_2O mixing ratios using EDGAR emissions were compared with measurements, and the results are also summarized in Table 1. Compared with the results before inverse optimization, the fitting slopes from the final inversion are closer to unity for most of the months, and the RMS errors are reduced significantly. For March, the posterior fitting slopes from both EDGAR emission models

Table 1. Linear Analysis Results Before and After Inverse Optimization

		Winter		Spring		Summer		Fall		
		12–1[a]	2	3	4–5[a]	6–7[a]	8	9	10	11
Before Inverse										
E32[b]	Slope	0.32 ± 0.06	0.36 ± 0.07	0.16 ± 0.02	0.25 ± 0.04	0.33 ± 0.07	0.50 ± 0.54	0.29 ± 0.07	0.76 ± 0.18	0.84 ± 0.14
	RMSE[d]	2.18	1.44	0.81	0.82	0.82	0.62	1.02	0.57	0.85
E42[c]	Slope	0.42 ± 0.09	0.42 ± 0.08	0.12 ± 0.02	0.25 ± 0.06	0.30 ± 0.05	0.29 ± 0.43	0.26 ± 0.13	0.63 ± 0.22	0.93 ± 0.17
	RMSE	2.18	1.45	0.87	0.88	0.84	0.68	1.10	0.68	0.92
After Inverse										
E32	Slope	0.95 ± 0.05	0.86 ± 0.08	0.64 ± 0.08	0.84 ± 0.09	0.85 ± 0.13	0.85 ± 0.48	0.90 ± 0.13	1.00 ± 0.19	0.93 ± 0.06
	RMSE	0.63	0.61	0.38	0.38	0.43	0.45	0.38	0.47	0.35
E42	Slope	0.96 ± 0.07	0.94 ± 0.07	0.51 ± 0.05	0.93 ± 0.16	0.88 ± 0.12	0.68 ± 0.39	0.93 ± 0.16	1.02 ± 0.22	1.02 ± 0.07
	RMSE	0.77	0.55	0.42	0.43	0.47	0.41	0.43	0.48	0.42

[a]Data for April, July, and December are combined with those of May, June, and January respectively (a total of 9 months), due to missing measurements and fire period cuts.
[b]EDGAR32.
[c]EDGAR42.
[d]RMSE is in units of ppb.

are relatively low compared to those of the other months but do not limit our ability to interpret seasonal N_2O emissions. As will be discussed later, monthly inversion results are not different from those of seasonal inversions where posterior slopes for all seasons are near unity.

[16] In the final inversion, outlier points were removed following *Bergamaschi et al.* [2005]. The outlier removals vary with month, excluding 6–20% (mean removal rate = 11.1%) and 4–22% (mean = 13.6%) of the data used in the first inversion for the EDGAR32 and EDGAR42 models, respectively. These removal rates are comparable to the 12–14% rate in *Bergamaschi et al.* [2005]. In the final inversion, to solve for 9 × 13 unknowns (13 regions for each month) we used 313 and 304 observations for the EDGAR32 and EDGAR42 cases, respectively.

[17] Inferred N_2O emissions are reported by season and as a regional sum over Regions 6, 7 and 8 where reduction in the posterior uncertainty is significant (Figure 2). The annual posterior N_2O emission summed over the three regions is 11.5 ± 2.1 and 11. 6 ± 1.9 Tg CO_2 eq from the EDGAR32 and EDGAR42 emission models, respectively. Although the two emission maps have different spatial resolutions, the estimated regional emissions are consistent. As a sensitivity analysis, we performed inversions using 200% and 300% uncertainties in the *a priori* emission models in addition to the baseline prior uncertainty (100%). For EDGAR42, the annual posterior N_2O emissions for the three regions were 13.2 ± 2.7 and 13.1 ± 3.0 Tg CO_2 eq for the 200% and 300% uncertainties in the *a priori* emissions, respectively. The EDGAR32 case also showed a similar result with no significant difference in posterior N_2O emissions. Averaging over seasons, annual mean scaling factors from EDGAR32 are 2.4 ± 0.5, 2.1 ± 0.6, and 1.3 ± 0.8 for Regions 6, 7, and 8, respectively, consistent with those obtained with EDGAR42: 2.6 ± 0.6, 2.3 ± 0.5, 1.4 ± 0.7. Note that these scaling factors are obtained by comparing posterior emissions from each EDGAR model with the corresponding prior sum. This result suggests that estimated emissions are considerably greater than the EDGAR emission maps in Region 7 containing San Francisco Bay and surrounding urban areas. Estimated emissions are also significantly higher than the EDGAR emission maps in Region 6 containing the southern end of the Sacramento Valley, where a large fraction of N_2O emissions is expected from agriculture. While posterior uncertainties are reduced significantly in Regions 6 and 7 for all seasons, the uncertainty reduction in Region 8 is relatively small except for the winter period when footprints extend significantly to the south of the tower (see Figure 1).

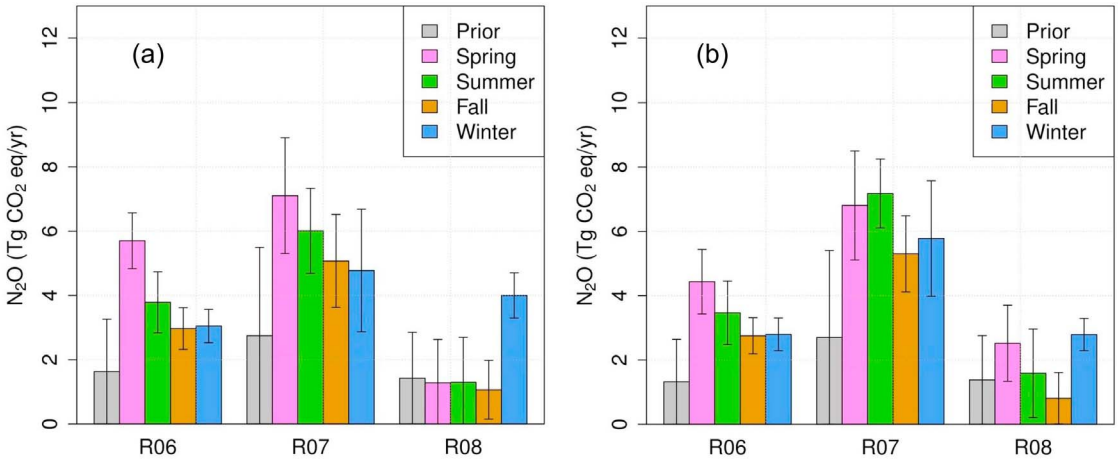

Figure 2. Posterior emission estimates for the three sensitive regions (uncertainty = 1σ): (a) EDGAR32 and (b) EDGAR42.

This suggests additional measurement stations are needed to constrain emissions in Region 8, which is likely an important sub-region in inferring emissions for livestock and crop agriculture.

[18] The posterior scaling factors show clear evidence of seasonal variation in N_2O emissions that is not captured in the EDGAR *a priori* models. Summing over Regions 6, 7 and 8, posterior seasonal emissions are 14.1 ± 2.4, 11.1 ± 2.2, 9.1 ± 1.8, 11.8 ± 2.1 Tg CO_2 eq yr^{-1} for spring, summer, fall, and winter, respectively, which are comparable to those of EDGAR42: 13.8 ± 2.3, 12.2 ± 2.0, 8.9 ± 1.5, and 11.4 ± 1.9 Tg CO_2 eq yr^{-1}. We compare this final inversion result from EDGAR32 with that of the first inversion, which yielded 17.1 ± 2.4, 12.0 ± 2.1, 9.6 ± 1.8, 13.0 ± 1.9 Tg CO_2 eq yr^{-1} for spring, summer, fall, and winter, respectively. There is no significant difference between the two inversions, and we found the same result for the EDGAR42 case. As a sensitivity analysis on the temporal scale, we used a seasonal temporal scale for inversion instead of the monthly scale used in our inversion. We found that the seasonal inversion with EDGAR32 was not significantly different from the monthly inversion, yielding posterior emission estimates of 13.6 ± 2.0, 13.2 ± 3.2, 8.5 ± 1.0, and 11.7 ± 1.0 Tg CO_2 eq yr^{-1}. The sensitivity analysis using a fixed value of 2 for α and EDGAR32 also showed no significant change in posterior emissions, yielding 14.3 ± 2.5, 11.3 ± 2.1, 10.0 ± 2.1 and 11.0 ± 2.2 Tg CO_2 eq yr^{-1}. These combined results indicate that posterior N_2O emissions for all seasons are significantly higher, compared to the annual EDGAR32 total (5.8 Tg CO_2 eq) or EDGAR42 total (5.4 Tg CO_2 eq) for Regions 6, 7 and 8.

[19] Figure 2 shows the seasonality in N_2O emissions in each sub-region. N_2O emissions from Region 6 based on both EDGAR emission models vary seasonally, showing largest emissions in spring and summer. Posterior emissions for Region 7 show seasonal variation where spring and summer emissions are higher than the other seasons. The EDGAR42 case also shows that summer and spring emissions are higher than the other seasons. For Region 8, seasonal variation in N_2O emissions is undetermined because of high posterior uncertainties although winter posterior emissions are significantly higher than EDGAR.

4. Discussion

[20] The N_2O emissions estimated in this study can be compared with those from other work for the Continental U.S. Spatially averaged N_2O emissions from Regions 6, 7 and 8 during late spring and early summer are 2.5 ± 0.4 times the EDGAR32 inventory. This is essentially consistent with results described in *Kort et al.* [2008], where N_2O emissions over a larger area of the U.S. and southern Canada were larger than the EDGAR32 inventory by a factor of 2.6 ± 0.5 for the May – June, 2003 period.

[21] Beyond the comparison for spring and summer, seasonal dynamics of N_2O emissions appear important for the mixture of urban, agricultural, and natural landscapes. Emissions for Central California in fall differ from EDGAR32 and EDGAR42 inventories by factors of 1.6 ± 0.3 and 1.6 ± 0.3, respectively, indicating that N_2O emissions vary by nearly 30% throughout the seasonal cycle.

[22] While it would be desirable to spatially resolve emissions, the footprints obtained for the single tower limit our ability to separate emissions from different sub-regions. This can be judged by the magnitude of cross-correlations between posterior emission estimates between different sub-regions [e.g., *Bergamaschi et al.*, 2005]. For our study, cross-correlations derived from the posterior covariance matrix were negative between Regions 6 and 7 (−0.6 to −0.1), with smaller anti-correlations between those regions and Region 8. This suggests that the large emissions in Region 7 in spring and summer can be traded off against emissions from Region 6 in a manner that cannot be uniquely resolved from the inversion system driven by data from a single tower [*Tarantola*, 1987].

[23] Putting our results in the context of California's total N_2O emissions requires an assumption about the spatial distribution of N_2O emissions. If the spatial distribution of EDGAR is applied across California using the mean estimated scaling factor from Regions 6, 7, and 8, then total N_2O emissions would be larger than the current state emission inventory by a factor of 2.7 ± 0.5, constituting 8.1 ± 1.4% of California's total estimated GHG emissions [*CARB*, 2012]. While there is no current evidence to suggest that the spatial distribution of N_2O emissions is incorrect, analysis of long-term measurements with footprints covering more of California is needed to improve the estimate of state total annual N_2O emissions.

[24] **Acknowledgments.** We thank the NOAA-ESRL staff for technical assistance, Los Gatos Research for loan of the in-situ N_2O instrument, John Lin, Steve Wofsy, Janusz Eluszkiewicz and Thomas Nehrkorn for generously sharing the STILT code, and two anonymous reviewers for valuable comments. We acknowledge NOAA Air Resources Laboratory (ARL) for the use of HYSPLIT underlying STILT, and NCEP for the provision of the NARR meteorology. This study was supported by the Public Interest Environmental Research Program of the California Energy Commission and Laboratory Directed Research and Development support from the Lawrence Berkeley National Laboratory under U.S. Department of Energy contract DE-AC02-05CH11231. The findings, views, and opinions presented in this paper do not represent the views and opinions of the California Energy Commission or the State of California.

[25] The Editor thanks two anonymous reviewers for assisting in the evaluation of this paper.

References

Bergamaschi, P., M. Krol, F. Dentener, A. Vermeulen, F. Meinhardt, R. Graul, M. Ramonet, W. Peters, and E. J. Dlugokencky (2005), Inverse modelling of national and European CH_4 emissions using the atmospheric zoom model TM5, *Atmos. Chem. Phys.*, *5*, 2431–2460, doi:10.5194/acp-5-2431-2005.

California Air Resources Board (CARB) (2012), *California greenhouse gas emission inventory*, report, Sacramento, Calif. [Available at http://www.arb.ca.gov/cc/inventory/inventory.htm.]

Corazza, M., et al. (2011), Inverse modelling of European N_2O emissions: Assimilating observations from different networks, *Atmos. Chem. Phys.*, *11*, 2381–2398, doi:10.5194/acp-11-2381-2011.

Gerbig, C., J. Lin, S. Wofsy, B. Daube, A. E. Andrews, B. Stephens, P. S. Bakwin, and C. Grainger (2003), Toward constraining regional-scale fluxes of CO_2 with atmospheric observations over a continent: 2. Analysis of COBRA data using a receptor-oriented framework, *J. Geophys. Res.*, *108*(D24), 4757, doi:10.1029/2003JD003770.

Göckede, M., A. M. Michalak, D. Vickers, D. P. Turner, and B. E. Law (2010), Atmospheric inverse modeling to constrain regional-scale CO_2 budgets at high spatial and temporal resolution, *J. Geophys. Res.*, *115*, D15113, doi:10.1029/2009JD012257.

Hall, B. D., G. S. Dutton, and J. W. Elkins (2007), The NOAA nitrous oxide standard scale for atmospheric observations, *J. Geophys. Res.*, *112*, D09305, doi:10.1029/2006JD007954.

Hirsch, A. I., A. M. Michalak, L. M. Bruhwiler, W. Peters, E. J. Dlugokencky, and P. P. Tans (2006), Inverse modeling estimates of the global nitrous oxide surface flux from 1998–2001, *Global Biogeochem. Cycles*, *20*, GB1008, doi:10.1029/2004GB002443.

Hofmann, D. J., J. H. Butler, E. J. Dlugokencky, J. W. Elkins, K. Masarie, S. A. Montzka, and P. Tans (2006), The role of carbon dioxide in climate

forcing from 1979–2004: Introduction of the Annual Greenhouse Gas Index, *Tellus, Ser. B*, *58*, 614–619, doi:10.1111/j.1600-0889.2006.00201.x.

Huang, J., et al. (2008), Estimation of regional emissions of nitrous oxide from 1997 to 2005 using multinetwork measurements, a chemical transport model, and an inverse method, *J. Geophys. Res.*, *113*, D17313, doi:10.1029/2007JD009381.

Intergovernmental Panel on Climate Change (1995), *Climate Change 1995: The Science of Climate Change. Contribution of Working Group I to the Second Assessment Report of the Intergovernmental Panel on Climate Change*, edited by J. T. Houghton et al., Cambridge Univ. Press, Cambridge, U. K.

Jeong, S., C. Zhao, A. E. Andrews, L. Bianco, J. M. Wilczak, and M. L. Fischer (2012), Seasonal variation of CH_4 emissions from central California, *J. Geophys. Res.*, *117*, D11306, doi:10.1029/2011JD016896.

Kort, E. A., J. Eluszkiewicz, B. B. Stephens, J. B. Miller, C. Gerbig, T. Nehrkorn, B. C. Daube, J. O. Kaplan, S. Houweling, and S. C. Wofsy (2008), Emissions of CH_4 and N_2O over the United States and Canada based on a receptor-oriented modeling framework and COBRA-NA atmospheric observations, *Geophys. Res. Lett.*, *35*, L18808, doi:10.1029/2008GL034031.

Lin, J. C., and C. Gerbig (2005), Accounting for the effect of transport errors on tracer inversions, *Geophys. Res. Lett.*, *32*, L01802, doi:10.1029/2004GL021127.

Lin, J. C., C. Gerbig, S. C. Wofsy, A. E. Andrews, B. C. Daube, K. J. Davis, and C. A. Grainger (2003), A near-field tool for simulating the upstream influence of atmospheric observations: The Stochastic Time-Inverted Lagrangian Transport (STILT) model, *J. Geophys. Res.*, *108*(D16), 4493, doi:10.1029/2002JD003161.

Montzka, S. A., E. J. Dlugokencky, and J. H. Butler (2011), Non-CO_2 greenhouse gases and climate change, *Nature*, *476*, 43–50, doi:10.1038/nature10322.

National Research Council (2010), *Verifying Greenhouse Gas Emissions: Methods to Support International Climate Agreements*, Natl. Acad. Press, Washington, D. C.

Nehrkorn, T., J. Eluszkiewicz, S. C. Wofsy, J. C. Lin, C. Gerbig, M. Longo, and S. Freitas (2010), Coupled weather research and forecasting–stochastic time-inverted Lagrangian transport (WRF-STILT) model, *Meteorol. Atmos. Phys.*, *107*(1–2), 51–64, doi:10.1007/s00703-010-0068-x.

Olivier, J. G. J., J. A. Van Aardenne, F. Dentener, L. Ganzeveld, and J. A. H. W. Peters (2005), Recent trends in global greenhouse gas emissions: Regional trends and spatial distribution of key sources, in *Non-CO_2* Greenhouse Gases (NCGG-4), edited by A. van Amstel, pp. 325–330, Millpress, Rotterdam, Netherlands.

Park, S., et al. (2012), Trends and seasonal cycles in the isotopic composition of nitrous oxide since 1940, *Nat. Geosci.*, *5*, 261–265, doi:10.1038/ngeo1421.

Press, W. H., S. A. Teukolsky, W. T. Vetterling, and B. P. Flannery (1992), *Numerical Recipes in FORTRAN*, 2nd ed., Cambridge Univ. Press, Cambridge, U. K.

Skamarock, W. C., J. B. Klemp, J. Dudhia, D. O. Gill, D. M. Barker, W. Wang, and J. G. Powers (2005), A description of the advanced research WRF version 2, *NCAR Tech. Note 468+STR*, Natl. Cent. for Atmos. Res., Boulder, Colo.

Tarantola, A. (1987), *Inverse Problem Theory Methods for Data Fitting and Model Parameter Estimation*, 613 pp., Elsevier, New York.

Zhao, C., A. E. Andrews, L. Bianco, J. Eluszkiewicz, A. Hirsch, C. MacDonald, T. Nehrkorn, and M. L. Fischer (2009), Atmospheric inverse estimates of methane emissions from central California, *J. Geophys. Res.*, *114*, D16302, doi:10.1029/2008JD011671.